High-Resolution Spectroscopic Investigation of the $\tilde{B}^2A_1-\tilde{X}^2A_1$ Transitions of $CaCH_3$ and $SrCH_3$

P. M. Sheridan,[†] M. J. Dick,[‡] J.-G. Wang,[†] and P. F. Bernath*[,†,‡]

Departments of Chemistry and Physics, University of Waterloo, Waterloo, Ontario N2L 3G1, Canada

Received: July 29, 2005; In Final Form: September 17, 2005

High-resolution spectra of the $\tilde{B}^2A_1-\tilde{X}^2A_1$ transitions of $CaCH_3$ and $SrCH_3$ have been recorded in a molecular jet/laser ablation source using laser excitation spectroscopy. Transitions arising from the $K = 0$ and 1 subbands have been observed for both molecules. An analysis of the data using a $^2A_1$ symmetric top Hamiltonian has determined rotational and spin-rotation constants for the $\tilde{B}^2A_1$ state of each molecule. From the rotational constants, structures have been estimated for both $CaCH_3$ and $SrCH_3$. The spin-rotation constant, $\epsilon_{bc} = (\epsilon_{bb} + \epsilon_{cc})/2$, in the $\tilde{B}^2A_1$ state for both molecules is in reasonable agreement with the value calculated using the pure precession approximation. For $CaCH_3$, the $K' = 1$ levels of the $\tilde{B}^2A_1$ state exhibit a perturbation that interchanges the energy ordering of the spin-rotation components.

1. Introduction

Metal-containing polyatomic compounds are ubiquitous in science. They are used in chemistry, where for example they play a significant role in catalysis and organic synthesis.[1,2] In biology, they exist in the active sites of enzymes whose functions are vital to life on earth.[3] In astrophysics, they play a critical role in understanding the composition and spectral energy distribution of cool stellar objects.[4,5] Because of their intrinsic importance, there has been a large effort to better understand the properties of these molecules. One approach has focused on examining the fundamental components of such species, that is, a metal atom bonded to a single ligand. One such example, the metal monomethyls (MCH_3), have been the subject of much research. The alkali, alkaline-earth, group 13, and transition metal monomethyls have been studied quite extensively using both experimental and theoretical methods.

Theoretical studies of metal monomethyl species greatly outnumber experimental investigations. A variety of methods have been used to examine the electronic structure, chemical reactivity, and spectroscopic parameters of many MCH_3 molecules. By far, the monomethyls of the alkali and alkaline-earth metals $LiCH_3$,[6−9] $NaCH_3$,[6,7,9] KCH_3,[7] $BeCH_3$,[10] $MgCH_3$,[10−13] $CaCH_3$,[10,14−16] and $SrCH_3$[14] and the group 13 metals $AlCH_3$[17] and $GaCH_3$[18] have received the greatest attention. For most of the transition metals, investigations have been limited to the comprehensive work of Bauschlicher and co-workers[19] in which metal−carbon bond dissociation energies as well as geometries for all of the first- and second-row transition metal monomethyls and their positive ions were calculated. Only a few theoretical studies exist for individual transition metal species, for example, $ZnCH_3$,[20−22] $NiCH_3$,[23] and $FeCH_3$.[24]

The metal monomethyls have also been studied by a wide array of experimental techniques. Mass spectrometric studies have been used to detect alkyl aluminum fragments such as $AlCH_3$.[25,26] The electronic and vibrational structures of $CrCH_3$ and $NiCH_3$[27] have been probed using resonant two-photon ionization spectroscopy. Ion beam studies have been used to measure the dissociation energies of the reaction products of transition metals with alkanes, such as $CoCH_3$[28] and $MnCH_3$.[29] A variety of laser excitation experiments including fluorescence depletion (FDS), zero electron kinetic energy (ZEKE) photoelectron, and resonance-enhanced multiphoton ionization (REMPI) spectroscopies have been used to characterize $ZnCH_3$ and $CdCH_3$.[30−37] In addition, Ziurys and co-workers have measured pure rotational spectra of many of these species using millimeter-wave spectroscopy. Their studies have included the monomethyls of Li, Na, K, Al, and Cu.[38−42] They also determined the first r_0 structures for Li, K, and Cu monomethyls[40,42] by recording the spectra of several isotopologues.

The main focus of this work has centered on further investigations of the alkaline-earth monomethyls. The first species to be observed were $CaCH_3$ and $SrCH_3$ by the Bernath group.[43] In their work, they recorded low-resolution spectra of the $\tilde{A}^2E-\tilde{X}^2A_1$ and $\tilde{B}^2A_1-\tilde{X}^2A_1$ transitions and performed a vibrational analysis by laser spectroscopy. Subsequently, high-resolution spectra of the $\tilde{A}^2E-\tilde{X}^2A_1$ transition of $CaCH_3$[44,45] were measured and rotational and fine structure parameters were determined from them. This study was followed by the detection of $MgCH_3$ via high-resolution laser excitation spectroscopy of the $\tilde{A}^2E-\tilde{X}^2A_1$ transition[46] and additional investigations of the rovibronic structure and bonding in this molecule.[31,47] The pure rotational spectra of the main isotopologues of these three species, as well as $BaCH_3$, have been measured using millimeter-wave spectroscopy.[48−51] Also, hyperfine structure in $CaCH_3$ has been observed by the pump/probe microwave-optical double resonance (PPMODR) technique.[52] Despite these numerous studies, the $\tilde{B}^2A_1$ state has not yet been examined at high resolution for any of the alkaline-earth monomethyls. To further investigate the low-lying states of the alkaline-earth metal monomethyls, we initiated a high-resolution study of the $\tilde{B}^2A_1-\tilde{X}^2A_1$ electronic transitions of $CaCH_3$ and $SrCH_3$. From our analysis of the high-resolution spectra, rotational and fine structure parameters have been determined for the $\tilde{B}^2A_1$ state for the first time. A comparison of the structure of these alkaline-earth monomethyls in their low-lying electronic states and of

* Corresponding author. Phone: 519-888-4814. Fax: 519-746-0435. E-mail: bernath@uwaterloo.ca.
[†] Department of Chemistry.
[‡] Department of Physics.

10.1021/jp054228q CCC: $30.25
Published on Web 11/02/2005

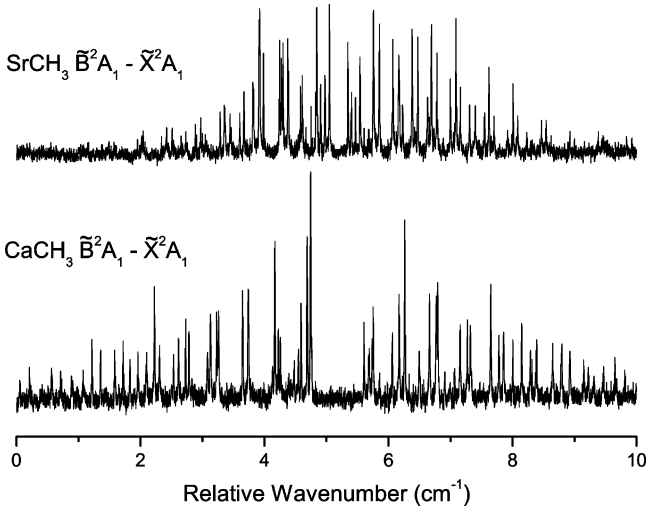

Figure 1. Overall high-resolution spectra of the $\tilde{B}^2A_1-\tilde{X}^2A_1$ transition of $SrCH_3$ (top panel) and $CaCH_3$ (bottom panel) plotted on a relative wavenumber axis for comparison. Both spectra have the appearance of parallel transitions. For $SrCH_3$, the rotational structure appears more condensed than in $CaCH_3$ due to the smaller rotational constant. Near the origin, a larger gap is observed in the spectrum of $CaCH_3$ than that for $SrCH_3$.

the fine structure constants in the $\tilde{B}^2A_1$ state in terms of the pure precession approximation will be presented.

2. Experimental Section

$SrCH_3$ and $CaCH_3$ were synthesized using the laser ablation/molecular jet source of the Bernath group.[53] The third harmonic (355 nm) of a pulsed (10 Hz) Nd:YAG laser (10 mJ/pulse) was used to vaporize either a calcium or strontium metal target rod. Using a gas mixture of 1% tetramethyltin in Ar, at a backing pressure of 100 psi, a free jet expansion was formed following the reaction of the hot metal atoms with the gas mixture. Rotationally cooled (4−6 K) $CaCH_3$ and $SrCH_3$ molecules were interrogated by a probe laser ∼15 cm downstream. The resulting laser induced fluorescence was collected using a photomultiplier tube, with the plasma radiation from the ablation source attenuated using band-pass filters (±20 nm). The signal was sent through a preamplifier (100× current) and then processed by a boxcar integrator.

A Coherent 699-29 ring dye laser system was used to obtain high-resolution spectra of the $\tilde{B}^2A_1-\tilde{X}^2A_1$ transitions of $CaCH_3$ and $SrCH_3$ (line width ∼10 MHz). The I_2 spectrum, recorded simultaneously with the experimental data, was used to calibrate the line positions.[54] Spectra were typically obtained in 5 cm^{-1} segments at a scan speed of 180 s/cm^{-1} with a spectral data sampling interval of 10 MHz. For $CaCH_3$, up to four 5 cm^{-1} scan segments (obtained on the same day) were averaged together in order to increase the signal-to-noise ratio. Experimental line widths were ∼350 MHz, a result of residual Doppler broadening in the molecular jet.

3. Results

High-resolution spectra of the $\tilde{B}^2A_1-\tilde{X}^2A_1$ transitions of $CaCH_3$ and $SrCH_3$ were recorded using the previous low-resolution investigation[43] as a guide. The overall spectrum for each molecule is plotted in Figure 1 ($SrCH_3$ on top; $CaCH_3$ on bottom) on a relative wavenumber axis for comparison. The spectra exhibit a pattern typical for a Hund's case (b) $^2\Sigma$ − Hund's case (b) $^2\Sigma$ parallel type transition, with line spacings of ∼2*B*. Because the $^2A_1$ electronic term correlates to a $^2\Sigma^+$ term in the linear limit,[55] this pattern is expected. At first glance, each spectrum has a similar appearance with well-defined P and R branches. However, upon closer examination, the origin area appears different between the two spectra; in $CaCH_3$, a larger gap is observed, suggesting the Q branch transitions have been shifted.

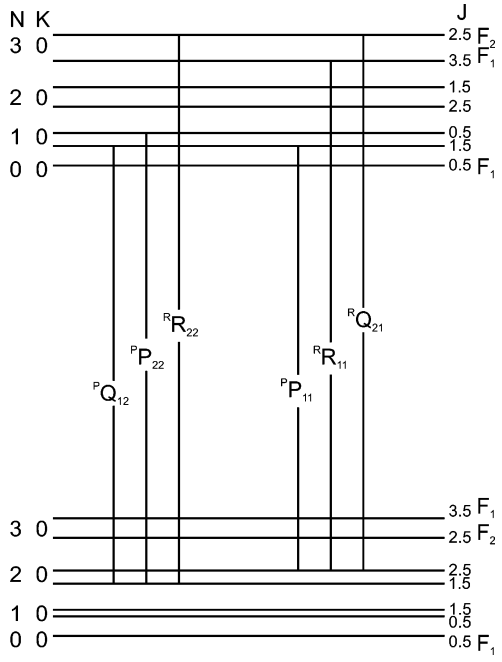

Figure 2. Energy level diagram of the $K = 0$ sub-band of the $\tilde{B}^2A_1-\tilde{X}^2A_1$ transition of $CaCH_3$ and $SrCH_3$. The rotational energy levels are labeled by the symmetric top quantum numbers *N*, *K*, and *J*. Each level is split into two fine structure components by the spin-rotation interaction and labeled as F_1 ($J = N + 1/2$) and F_2 ($J = N - 1/2$). Transitions arising from the six possible branches are shown and identified by the branch notation $^{\Delta N}\Delta J_{F_i'F_j''}$ ($i = 1, 2$; $j = 1, 2$). The structure of this sub-band resembles a Hund's case (b) $^2\Sigma$ − Hund's case (b) $^2\Sigma$ transition.

$SrCH_3$ and $CaCH_3$ are prolate symmetric top molecules and belong to the C_{3v} point group. The dipole moment lies along the *a* molecular axis (metal−carbon bond); therefore, the selection rule $\Delta K = 0$ results and transitions can be grouped into sub-bands labeled by *K*, the projection of the rotational angular momentum (*N*) on the symmetry axis. Rotation of the molecule about the *a* axis exchanges the three methyl protons and gives rise to two nuclear spin states: ortho ($K = 3N$, where *N* is an integer) and para ($K \neq 3N$).[56] The primary effect of these nuclear spin states is to enhance the intensity of the $K'' = 1$ levels beyond what is expected for normal collisional cooling because para states cannot cool to ortho states or vice versa in the free jet expansion. As a result, $K'' = 0$ (ortho) and $K'' = 1$ (para) levels of the $\tilde{X}^2A_1$ state are populated in our molecular jet and transitions originating from both levels are expected to be readily observed in our spectra. Nuclear spin statistics also enhance the intensity of the ortho levels relative to the para levels by a factor of 2 (all else being equal).

Energy level diagrams of the $K = 0$ and 1 sub-bands of the $\tilde{B}^2A_1-\tilde{X}^2A_1$ transition are presented in Figures 2 and 3, respectively. Because of the presence of an unpaired electron, each rotational energy level is split into two spin-rotation components labeled by F_1 ($J = N + 1/2$) and F_2 ($J = N - 1/2$). For the $K = 0$ sub-band (Figure 2), the selection rule $\Delta J = \Delta N = \pm 1$ gives rise to two P and R branches and $\Delta J = 0$, $\Delta N = \pm 1$ results in two satellite Q branches. The resulting branch structure resembles a Hund's case (b) $^2\Sigma$ − Hund's case (b) $^2\Sigma$

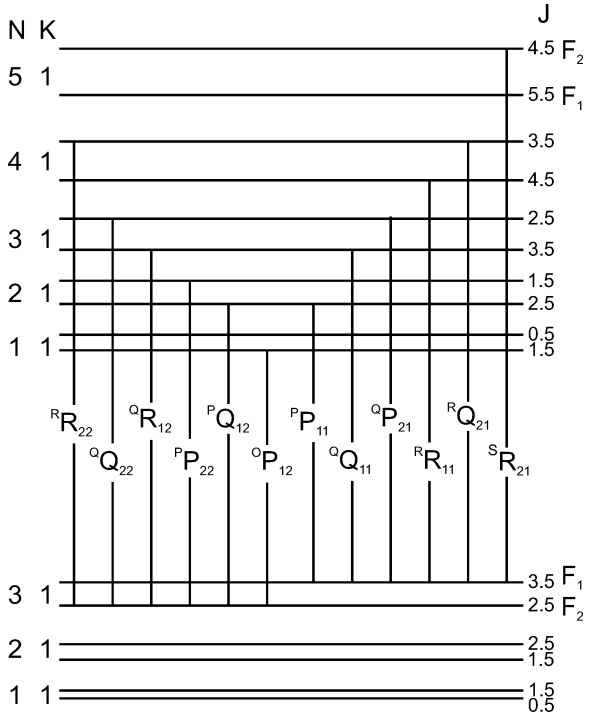

Figure 3. Energy level diagram showing the allowed transitions of the $K = 1$ sub-band of the $\tilde{B}^2A_1-\tilde{X}^2A_1$ transition of $CaCH_3$ and $SrCH_3$. Again, each rotational level is labeled by the symmetric top quantum numbers N, K, and J. Twelve branches are possible, labeled as ${}^{\Delta N}\Delta\mathbf{J}_{F_iF_j''}$ ($i = 1, 2$; $j = 1, 2$). The structure of this sub-band resembles a Hund's case (b) $^2\Pi$ − Hund's case (b) $^2\Pi$ transition.

transition. For the $K = 1$ sub-band (Figure 3), three main branches (^{P}P, ^{Q}Q, and ^{R}R) arise from within each F_1 and F_2 spin component via the selection rule $\Delta J = \Delta N = 0, \pm 1$. In addition, six satellite branches ($\Delta J \neq \Delta N$; $\Delta J = 0, \pm 1$; $\Delta N = 0, \pm 1, \pm 2$) are possible. The overall branch structure for the $K = 1$ sub-band has the appearance of a Hund's case (b) $^2\Pi$ − Hund's case (b) $^2\Pi$ transition.

For $SrCH_3$, individual P and R branches were identified in the spectrum of the $\tilde{B}^2A_1-\tilde{X}^2A_1$ transition with little difficulty. Each branch was then assigned as arising from either the F_1 or F_2 spin component based on their relative line spacings, which differed due to the larger spin-rotation interaction in the $\tilde{B}^2A_1$ state than in the $\tilde{X}^2A_1$ state. Ground state combination differences, available from the millimeter-wave work,[50] were used to match the corresponding P and R branches across the origin and confirm the J assignments. Initially, the P and R branches of the $K = 0$ sub-band were added to the fitting program followed by those of the $K = 1$ sub-band. The remaining satellite and ^{Q}Q branches were then predicted, identified, and added to the fit. For the $\tilde{B}^2A_1-\tilde{X}^2A_1$ transition, 108 lines were measured and are listed in Supporting Information Table S1. Figure 4 shows a short section of the high-resolution spectrum of the $\tilde{B}^2A_1-\tilde{X}^2A_1$ transition of $SrCH_3$ with these branch assignments. Transitions arising from the $K = 0$ sub-band are labeled on top in italics, while those from the $K = 1$ sub-band are labeled below. The effect of the larger spin-rotation interaction in the $\tilde{B}^2A_1$ state is apparent in the line spacings observed; for example, the $^{P}P_{11}$ and $^{R}R_{22}$ branches possess a greater spacing than the $^{P}P_{22}$ and $^{R}R_{11}$ branches. The $\Delta N = 0$ branches of the $K = 1$ sub-band are found near the origin, each exhibiting an evenly spaced pattern of lines with J values increasing in the direction away from the origin.

Initially, line assignments of the $\tilde{B}^2A_1-\tilde{X}^2A_1$ transition of $CaCH_3$ were made following the method outlined for $SrCH_3$.

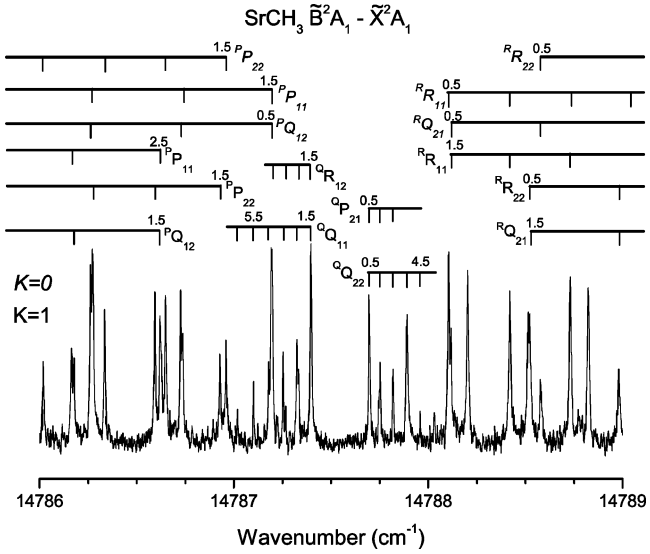

Figure 4. Subsection of the $\tilde{B}^2A_1-\tilde{X}^2A_1$ spectrum of $SrCH_3$ near the origin shown with branch assignments. Transitions belonging to the $K = 0$ sub-band are labeled on top in italics, while those arising from the $K = 1$ sub-band are shown below. Individual lines are labeled by their J values. Two different spacings are present in the branch structure due to the larger spin-rotation interaction in the $\tilde{B}^2A_1$ state as compared with the $\tilde{X}^2A_1$ state. In the $K = 1$ sub-band, the $\Delta N = 0$ branches are found near the band origin, each exhibiting an even line spacing as the J values increase in the direction away from the origin.

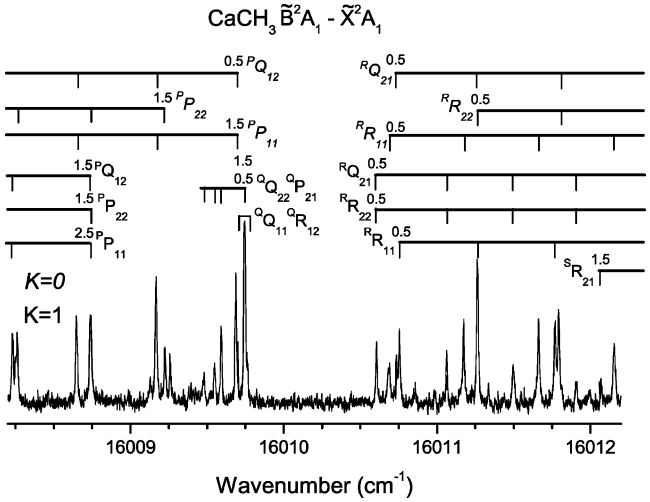

Figure 5. For $CaCH_3$, a subsection of the $\tilde{B}^2A_1-\tilde{X}^2A_1$ spectrum is shown near the origin with branch assignments. Individual lines are labeled by their J values. Transitions belonging to the $K = 0$ sub-band are identified on top (in italics) and have a similar appearance to the $K = 0$ sub-band of $SrCH_3$. The line spacing in the $K = 1$ sub-band has a different appearance than that in the $K = 0$ sub-band, and each branch is shifted to lower wavenumbers. In addition, the $\Delta N = 0$ branches appear condensed with $^{Q}Q_{22}$ and $^{Q}P_{21}$ exhibiting an uneven line spacing.

Main and satellite branch transitions of the $K = 0$ sub-band were first identified and added to the fit. However, the remaining unassigned features did not exhibit a similar spectral pattern as observed for the $K = 1$ sub-band of $SrCH_3$. Although these lines could be grouped into branches, their relative spacings did not resemble those observed in the $K = 0$ sub-band, making assignment of the F_1 and F_2 spin components difficult. Also, as mentioned previously, no clear $\Delta N = 0$ transitions ($^{Q}Q_{11}$, $^{Q}Q_{22}$, $^{Q}R_{12}$, and $^{Q}P_{21}$ branches) were found in the origin region, although a condensed area of lines was observed at lower wavenumbers. Despite these differences, quantum numbers were finally assigned to the remaining features using lower state

TABLE 1: Spectroscopic Constants (in cm^{-1}) for the $\tilde{B}^2A_1$ and $\tilde{X}^2A_1$ States of $CaCH_3$ and $SrCH_3$

	$CaCH_3$		$SrCH_3$	
constant[a]	$\tilde{X}^2A_1$	$\tilde{B}^2A_1$	$\tilde{X}^2A_1$	$\tilde{B}^2A_1$
T	0.0	16 010.195 25(60)	0.0	14 787.581 34(64)
A	5.448 31[b]		5.390[c]	5.309 29(84)
B	0.252 384 873(17)	0.253 254 2(98)	0.193 833 336(16)	0.193 603(14)
D_N	$3.544\,82(19) \times 10^{-7}$		$2.148\,93(11) \times 10^{-7}$	
D_{NK}	$1.995\,55(21) \times 10^{-5}$		$1.613\,49(51) \times 10^{-5}$	$5.3(1.8) \times 10^{-5}$
H_{NK}	$4.044(23) \times 10^{-10}$		$2.920(22) \times 10^{-10}$	
H_{KN}	$3.520(21) \times 10^{-9}$		$3.19(43) \times 10^{-9}$	
ϵ_{aa}	0.000 218 7(73)		0.000 884(35)	−0.252 2(21)
ϵ_{bc}	0.001 852 14(37)	−0.035 77(12)	0.004 128 53(44)	−0.148 78(11)

[a] Values in parentheses are 1σ standard deviations, in units of the last significant digits. [b] Fixed to experimental value.[44] [c] Fixed to theoretical value.[14]

combination differences.[49] For the $\tilde{B}^2A_1-\tilde{X}^2A_1$ transition, 132 lines were measured and are listed in Supporting Information Table S2. Figure 5 shows a subsection of the $\tilde{B}^2A_1-\tilde{X}^2A_1$ spectrum of $CaCH_3$. As mentioned before, the structure of the $K = 0$ sub-band (labeled on top in italics) appears similar to that observed for $SrCH_3$. For the $K = 1$ sub-band (labeled on bottom), each branch appears shifted to lower wavenumbers relative to the $K = 0$ sub-band. All $\Delta N = 0$ branches appear condensed, with the $^QQ_{22}$ and $^QP_{21}$ branches exhibiting an uneven spacing. The red shift of the $K = 1$ sub-band suggests a perturbation in the $K' = 1$ levels of the $\tilde{B}^2A_1$ state as the $K'' = 1$ levels of the $\tilde{X}^2A_1$ state[49,52] appear to be unperturbed.

4. Analysis

The data recorded for the $\tilde{B}^2A_1-\tilde{X}^2A_1$ transitions of $CaCH_3$ and $SrCH_3$ were fit using an appropriate effective Hamiltonian to model each $^2A_1$ state of the form[46,50,57]

$$\hat{H}_{Eff} = \hat{H}_{Rot} + \hat{H}_{CD} + \hat{H}_{SR} \quad (1)$$

In the above expression, $\hat{H}_{Rot}$ describes the rotational motion, $\hat{H}_{CD}$ contains centrifugal distortion terms, and $\hat{H}_{SR}$ accounts for the spin-rotation fine structure interaction. The energy separation between the lowest rotational levels of each state is given by T. Using the fitting program developed by Pickett,[58] a least-squares fit of the experimental data to the Hamiltonian in eq 1 was performed. For $SrCH_3$, the data set included all lines arising from the $K = 0$ and $K = 1$ sub-bands ($J \leq 10.5$) and the pure rotational data,[50] which was included to obtain proper experimental errors. The two data sets were weighted according to their experimental uncertainties: for the optical transitions, 0.003 cm^{-1} was employed, while, for the pure rotational data, a value of 60 kHz was used. Values of the spectroscopic constants determined in the final fit for the $\tilde{B}^2A_1$ and $\tilde{X}^2A_1$ states of $SrCH_3$ are listed in Table 1 (note that $\epsilon_{bc} = (\epsilon_{bb} + \epsilon_{cc})/2$).[46] The ground state $\tilde{X}^2A_1$ parameters in our fit differ slightly from the millimeter-wave work because we chose to fit ϵ_{aa} and fix the centrifugal distortion constant D_K and the spin-rotation centrifugal distortion constants D_{NKS} and D_{NS} to zero. These changes produced residuals better than those previously reported and are similar to the changes made in the refit of the millimeter-wave data of $CaCH_3$ in the subsequent PPMODR study[52] of this molecule. In addition, the A rotational constant in the ground state was fixed to the theoretical value.[14] For the $\tilde{B}^2A_1$ state, the values of the B rotational constant, the centrifugal distortion constant D_{NK}, and the spin-rotation constant ϵ_{bc} were determined. Because transitions from the $K = 1$ sub-band were included in the fit, the A rotational constant (actually ΔA) as well as ϵ_{aa} could be ascertained.

TABLE 2: Structural Parameters for Alkaline-Earth Monomethyls

state	parameter	$CaCH_3$	$SrCH_3$[a]
$\tilde{X}^2A_1$	r_{M-C} (Å)	2.348	2.487
	r_{C-H}[b] (Å)	1.102	1.104
	θ_{H-C-H} (deg)	105.3	105.8
$\tilde{A}^2E$	r_{M-C} (Å)	2.342	
	r_{C-H}[b] (Å)	1.102	
	θ_{H-C-H} (deg)	106.2	
$\tilde{B}^2A_1$	r_{M-C} (Å)	2.348[c]	2.492
	r_{C-H}[b] (Å)	1.102	1.104
	θ_{H-C-H} (deg)	106.6	107.0

[a] Value of A in ground state fixed to theoretical value.[14] [b] Fixed to theoretical value.[14] [c] Fixed to ground state value.

For $CaCH_3$, transitions arising from only the $K = 0$ sub-band were included in the final fit using the same weighting factors as those used for $SrCH_3$. All attempts to include data from the $K = 1$ sub-band failed because of the perturbation. The pure rotational transitions of $CaCH_3$[49] were included in the final fit. The spectroscopic parameters derived from the fit of the data for the $\tilde{B}^2A_1$ and $\tilde{X}^2A_1$ states of $CaCH_3$ are also listed in Table 1. The ground state constants are in good agreement with those reported in the PPMODR work.[52] The A rotational constant was fixed to the experimentally determined value in the analysis of the $\tilde{A}^2E-\tilde{X}^2A_1$ transition.[44] For the $\tilde{B}^2A_1$ state, only B and ϵ_{bc} could be determined from the limited data set.

5. Discussion

A. Structure and Bonding. The structures of $CaCH_3$ and $SrCH_3$ in the $\tilde{B}^2A_1$ states can be estimated using the rotational constants derived in this study. Table 2 contains the known geometric parameters for the $\tilde{X}^2A_1$, $\tilde{A}^2E$, and $\tilde{B}^2A_1$ states of these molecules. Unfortunately, no relevant isotopologue data are available for these species; therefore, at least one structural parameter was assumed in each state. Because the C−H bond length should exhibit the smallest change upon electronic excitation, as in $CaOCH_3$,[59] this parameter was fixed to the ground state theoretical value in each state for each molecule. For $SrCH_3$, an additional assumption was made by using the theoretical value of the A rotational constant in the $\tilde{X}^2A_1$ state. For $CaCH_3$, no additional assumptions in the $\tilde{A}^2E$ and $\tilde{X}^2A_1$ states were necessary, as A was determined experimentally in the previous optical analysis. In the $\tilde{B}^2A_1$ state, the metal−carbon bond length was fixed to the ground state value, since A could not be determined.

To extract structural information from the rotational constants in the excited states of calcium and strontium monomethyl, second-order spin−orbit contributions to these parameters need to be considered. For the A rotational constant of the $\tilde{A}^2E$ state of $CaCH_3$, second-order contributions were found to comprise

only ~0.35% of its total value.[45] Similarly, for the *A* and *B* rotational constants of the $\tilde{B}^2A_1$ states of $CaCH_3$ and $SrCH_3$, the effect was calculated to be less than 0.1% of these parameters. Therefore, differences observed between the rotational constants in the excited states of $CaCH_3$ and $SrCH_3$ are due to structural changes. In the structure determination of $CaOCH_3$,[59] second-order contributions to the rotational constants were also found to be negligible.

Although the geometric parameters for $CaCH_3$ and $SrCH_3$ listed in Table 2 are based on several assumptions, they provide a reasonable estimate of the metal−carbon bond length in these low-lying electronic states. For $CaCH_3$, the metal−carbon bond length increases ~0.006 Å from the $\tilde{X}^2A_1$ state (sσ orbital) to the $\tilde{A}^2E$ state (pπ orbital), while, for $SrCH_3$, the metal−carbon bond length exhibits a small increase (0.005 Å) between the $\tilde{X}^2A_1$ and $\tilde{B}^2A_1$ (pσ orbital) electronic states. For calcium and strontium polyatomic radicals (MOH, MCCH, MNH_2, and $MOCH_3$), the metal−ligand bond length has typically been observed to decrease by >0.01 Å upon excitation from the ground state to similar low-lying electronic states.[57,59−63] This bond length shortening has been rationalized by the effect of the unpaired electron (pσ or pπ) being polarized away from the ligand in these states, allowing for a greater electrostatic interaction between the metal cation and the anionic ligand. This occurs regardless of the ligand, as the unpaired electron is located on the metal center. Using simple molecular orbital theory, the bond length behavior of these calcium and strontium polyatomics can be explained. The energy overlap of the metal and ligand orbitals that form the σ bond decreases as one goes from CH_3 to CCH to NH_2 to OH. Therefore, among these ligands, the metal−carbon bond in MCH_3 can be considered the most covalent in character and the metal−oxygen bond in MOH the least. In the highly ionic hydroxides, an increase in the metal−ligand electrostatic interaction upon excitation is expected to have a greater effect in shortening the bond length than in the more covalent monomethyls.

B. Pure Precession in $CaCH_3$ and $SrCH_3$. It has been shown that the spin-rotation fine structure interaction is composed of two main contributions: a first-order direct interaction and a second-order part due to spin−orbit coupling.[64] For molecules containing heavy atoms, the second-order term generally dominates. An expression for the second-order spin−orbit coupling contribution has been given by Dixon[65] for a nonlinear molecule. This equation can be simplified using the pure precession approximation, in which the interacting electronic states are described by single individual electronic configurations that differ by only one spin−orbital. If the unique perturber approximation is also invoked (a single perturbing state is assumed), then an expression for the ϵ_{bc} spin-rotation constant can be derived for the $\tilde{B}^2A_1$ state of $CaCH_3$ and $SrCH_3$:[57]

$$\epsilon_{bc} = \frac{4BA^{so}}{E_{\tilde{A}} - E_{\tilde{B}}} \qquad (2)$$

where *B* is the rotational constant ($\tilde{B}$ state), A^{so} is the spin−orbit constant for a linear analogue, and $E_{\tilde{A}}$ and $E_{\tilde{B}}$ are the energies of the $\tilde{A}^2E$ and $\tilde{B}^2A_1$ states, respectively. Using the A^{so} values for the corresponding hydroxides (CaOH,[66] 66.2 cm^{-1}; SrOH,[67] 263.5 cm^{-1}) and $E_{\tilde{A}}$ values for $CaCH_3$[46] and $SrCH_3$[43] of 14 743.4 and 13 789.5 cm^{-1}, ϵ_{bc} is calculated to be −0.0529 and −0.2044 cm^{-1} for $CaCH_3$ and $SrCH_3$, respectively. The experimental values are approximately 70% smaller than the calculated values, and in both cases, the signs are in agreement with the calculation. Deviations between the experimental and calculated values most likely arise from the simple assumptions involved in obtaining eq 2. For example, the unpaired electron in the $\tilde{B}^2A_1$ state is most likely not completely p in character; some metal d character is very likely present.

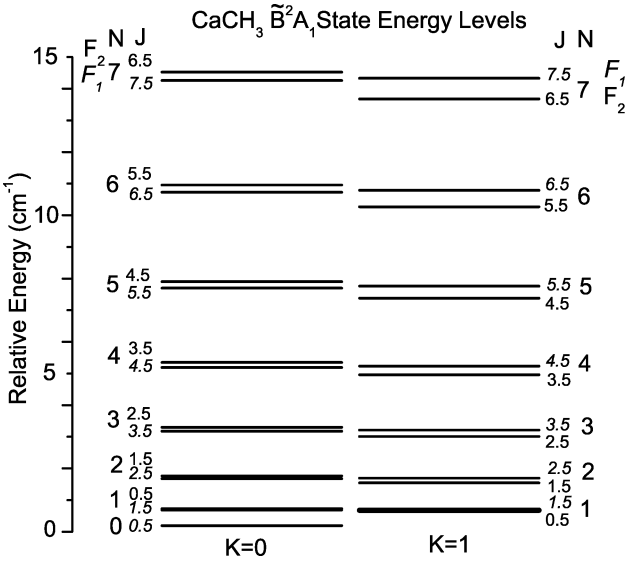

Figure 6. Term values of the rotational energy levels of the $K' = 0$ and 1 levels of the $\tilde{B}^2A_1$ state of $CaCH_3$ plotted on a relative energy scale. Each level is labeled by the quantum numbers *N* and *J*. In the $K' = 0$ levels, the F_2 spin component lies higher in energy than the F_1 spin component (in italics), as expected for a negative value of the ϵ_{bc} spin-rotation constant. In the $K' = 1$ levels, however, the F_2 spin component is pushed lower in energy than the F_1 spin component by a nearby perturbing state.

The pure precession and unique perturber approximations can also be used to derive a similar expression for the ϵ_{aa} spin-rotation parameter:[57]

$$\epsilon_{aa} = \frac{-4AA^{so}}{E_{^2A_2} - E_{\tilde{B}}} \qquad (3)$$

where *A* is the rotational constant ($\tilde{B}$ state). In this case, the interacting state is of $^2A_2$ symmetry; however, this state does not arise from either p or d atomic orbitals on the metal. This state most likely results from the ligand orbitals which become more important to bonding at higher energy.[57] Using the experimental value of ϵ_{aa} for $SrCH_3$, a $^2A_2$ state is predicted to lie at ~37 000 cm^{-1}. Theoretical calculations would be useful in confirming the existence of such a state and in predicting its properties. Unfortunately, because a value of ϵ_{aa} could not be obtained in the $\tilde{B}^2A_1$ state of $CaCH_3$, a comparison cannot be made with $SrCH_3$.

C. Perturbation in the $K' = 1$ Energy Levels in the $\tilde{B}^2A_1$ State of $CaCH_3$. As mentioned previously, the $K' = 1$ levels of the $\tilde{B}^2A_1$ state are perturbed and could not be fitted using the $^2A_1$ symmetric top Hamiltonian of eq 1. However, the lines of the $K = 1$ sub-band could be assigned quantum numbers using lower state combination differences[49] and term values obtained for the $K' = 1$ levels. To investigate the nature of the perturbation, these excited state term values for the $K = 1$ sub-band are plotted in Figure 6 on a relative energy scale alongside those of the $K = 0$ sub-band for comparison. The $K' = 0$ energy levels follow the expected ordering for a state with a negative value of the ϵ_{bc} spin-rotation parameter (as predicted by pure precession) in which the F_1 levels lie lower in energy than the F_2 levels and their separation increases with increasing *N*. The $K' = 1$ levels should exhibit a similar pattern, but this is not

the case. The relative energies of the F_1 levels do not change greatly between the $K' = 0$ and $K' = 1$ levels; however, the F_2 levels are clearly pushed down in energy so much that they are now below the F_1 levels. This effect is observed in all of the rotational levels observed in this study, which suggests that the perturbation is global in nature and affects primarily the F_2 levels of the $\tilde{B}^2A_1$ state of $CaCH_3$.

Considering the limited information available on the energy levels of $CaCH_3$, it is hard to identify the perturbing state with confidence. However, one possibility is that a vibrational level of the $\tilde{A}^2E$ state could be interacting with the $\tilde{B}^2A_1$ state ($\Delta E = 1267$ cm^{-1}). The vibrational frequency for the Ca−C stretch (υ_3) in the $\tilde{A}^2E$ state of $CaCH_3$ is ~413 cm^{-1}.[43] The energy of three quanta of this vibration in the $\tilde{A}^2E_{3/2}$ (14 779 cm^{-1}) F_2 spin component lies very close in energy to the $K' = 1$ level (~3 cm^{-1}) of the $\tilde{B}^2A_1$ state, while $3\upsilon_3$ in the $\tilde{A}^2E_{1/2}$ (14 700 cm^{-1}) F_1 spin component lies ~75 cm^{-1} below the $K' = 1$ level of the $\tilde{B}^2A_1$ state. The location of these levels matches the observation that the F_2 levels are more perturbed. More work will be necessary to confirm this possibility for the identity of the perturbing state. It would be very interesting to examine the $\tilde{B}^2A_1-\tilde{X}^2A_1$ transition of the $CaCD_3$ isotopologue to see if the perturbation changes as both the location of the electronic states and vibrational frequencies shift.

6. Conclusion

The $\tilde{B}^2A_1-\tilde{X}^2A_1$ electronic transitions of $CaCH_3$ and $SrCH_3$ have been rotationally analyzed using high-resolution laser excitation spectroscopy. Rotational and fine structure parameters have been determined for the $\tilde{B}^2A_1$ states of each molecule. From the rotational constants, structures have been estimated for the $\tilde{B}^2A_1$ states of $CaCH_3$ and $SrCH_3$. The spin-rotation parameters calculated for the $\tilde{B}^2A_1$ states using the pure precession approximation are in relatively good agreement with the experimentally determined values. Finally, the $K' = 1$ energy levels of the $\tilde{B}^2A_1$ state of $CaCH_3$ appear to be perturbed, possibly by an excited vibrational state ($3\upsilon_3$) of the metal−carbon stretch of the $\tilde{A}^2E$ state.

Acknowledgment. Financial support for this work was provided by the Natural Sciences and Engineering Research Council (NSERC) of Canada. In addition, the authors thank Dr. B. J. Drouin for his assistance in using Pickett's program.

Supporting Information Available: The $\tilde{B}^2A_1-\tilde{X}^2A_1$ electronic transition data for $CaCH_3$ and $SrCH_3$. This material is available free of charge via the Internet at http://pubs.acs.org.

References and Notes

(1) Cotton, F. A.; Wilkinson, G. W.; Murillo, C. A.; Bochmann, M. *Advanced Inorganic Chemistry*; Wiley: New York, 1999.
(2) Crabtree, R. H. *The Organometallic Chemistry of the Transition Metals*; Wiley-Interscience: New York, 2005.
(3) Voet, D.; Voet, J. G.; Pratt, C. W. *Fundamentals of Biochemistry*; Wiley: New York, 1999.
(4) Ziurys, L. M.; Savage, C.; Highberger, J. L.; Apponi, A. J.; Guélin, M.; Cernicharo, J. *Astrophys. J.* **2002**, *564*, L45.
(5) Highberger, J. L.; Ziurys, L. M. *Astrophys. J.* **2003**, *597*, 1065.
(6) Lambert, C.; Kaupp, M.; Schleyer, P. v. R. *Organometalics* **1993**, *12*, 853.
(7) Tyerman, S. C.; Corlett, G. K.; Ellis, A. M.; Claxton, T. A. *J. Mol. Struct.* **1996**, *364*, 107.
(8) Breidung, J.; Thiel, W. *J. Mol. Struct.* **2001**, *599*, 239.
(9) Scalmani, G.; Brédas, J. L.; Barone, V. *J. Chem. Phys.* **2000**, *112*, 1178.
(10) Jalbout, A. F. *Chem. Phys. Lett.* **2001**, *340*, 571.
(11) McKinley, A. J.; Karakyriakos, E. *J. Phys. Chem. A* **2000**, *104*, 8872.
(12) Drissi El Bouzaidi, R.; El Hammadi, A.; El Mouhtadi, M.; Cardy, H.; Dargelos, A. *J. Mol. Struct.* **2000**, *497*, 165.
(13) Woon, D. E. *J. Chem. Phys.* **1996**, *104*, 9495.
(14) Chan, W.-T.; Hamilton, I. P. *Chem Phys. Lett.* **1998**, *297*, 217.
(15) Ortiz, J. V. *J. Chem. Phys.* **1990**, *92*, 6728.
(16) El Hammadi, A.; El Mouhtadi, M.; Cardy, H.; Dargelos, A. *J. Mol. Struct.* **2003**, *624*, 1.
(17) Jin, S. Q.; Xie, Y.; Schaefer, H. F., III. *Chem. Phys. Lett.* **1990**, *170*, 301.
(18) Hoffman, B. C.; Sherrill, C. D.; Schaefer, H. F., III. *J. Mol. Struct.* **1996**, *370*, 93.
(19) Bauschlicher, C. W., Jr.; Langhoff, S. R.; Partridge, H.; Barnes, L. A. *J. Chem. Phys.* **1989**, *91*, 2399.
(20) Zakrzewski, V. G.; Ortiz, J. V. *J. Chem. Phys.* **1994**, *100*, 6508.
(21) McKinley, A. J.; Karakyriakos, E.; Knight, L. B., Jr.; Babb, R.; Williams, A. *J. Phys. Chem. A* **2000**, *104*, 3528.
(22) Jamorski, Ch.; Dargelos, A.; Teichteil, Ch.; Daudey, J. P. *Chem. Phys.* **1993**, *178*, 39.
(23) Rappe, A. K.; Goddard, W. A., III. *J. Am. Chem. Soc.* **1977**, *99*, 3966.
(24) Veldkamp, A.; Frenking, G. *J. Comput. Chem.* **1992**, *13*, 1184.
(25) Zhang, Y.; Stuke, M. *J. Phys. Chem.* **1989**, *93*, 4503.
(26) Srinivas, R.; Sülzle, D.; Schwarz, H.; *J. Am. Chem Soc.* **1990**, *112*, 8334.
(27) Brugh, D. J.; Dabell, R. S.; Morse, M. D. *J. Chem. Phys.* **2004**, *121*, 12379.
(28) Armentrout, P. B.; Beauchamp, J. L. *J. Am. Chem. Soc.* **1981**, *103*, 784.
(29) Sunderlin, L. S.; Armentrout, P. B. *J. Phys. Chem.* **1990**, *94*, 3589.
(30) Pushkarsky, M. B.; Barckholtz, T. A.; Miller, T. A. *J. Chem. Phys.* **1999**, *110*, 2016.
(31) Barckholtz, T. A.; Powers, D. E.; Miller, T. A.; Bursten, B. E. *J. Am. Chem. Soc.* **1999**, *121*, 2576.
(32) Panov, S. I.; Power, D. E.; Miller, T. A. *J. Chem. Phys.* **1998**, *108*, 1335.
(33) Penner, A.; Amirav, A. *Chem. Phys. Lett.* **1991**, *176*, 147.
(34) Robles, E. S. J.; Ellis, A. M.; Miller, T. A. *Chem. Phys. Lett.* **1991**, *178*, 185.
(35) Jackson, R. L. *Chem. Phys. Lett.* **1990**, *174*, 53.
(36) Cerny, T. M.; Tan X. Q.; Williamson, J. M.; Robles, E. S. J.; Ellis, A. M.; Miller, T. A. *J. Chem. Phys.* **1993**, *99*, 9376.
(37) Ellis, A. M.; Robles, E. S. J.; Miller, T. A. *Chem. Phys. Lett.* **1992**, *190*, 599.
(38) Allen, M. D.; Pesch, T. C.; Robinson, J. S.; Apponi, A. J.; Grotjahn, D. B.; Ziurys, L. M. *Chem. Phys. Lett.* **1998**, *293*, 397.
(39) Li, B.-Z.; Xin, J.; Ziurys, L. M. *Chem. Phys. Lett.* **1997**, *280*, 513.
(40) Grotjahn, D. B.; Pesch, T. C.; Brewster, M. A.; Ziurys, L. M. *J. Am. Chem. Soc.* **2000**, *122*, 4735.
(41) Robinson, J. S.; Ziurys, L. M. *Astrophys. J.* **1996**, *472*, L131.
(42) Grotjahn, D. B.; Halfen, D. T.; Ziurys, L. M.; Cooksy, A. L. *J. Am. Chem. Soc.* **2004**, *126*, 12621.
(43) Brazier, C. R.; Bernath, P. F. *J. Chem. Phys.* **1987**, *86*, 5918.
(44) Brazier, C. R.; Bernath, P. F. *J. Chem. Phys.* **1989**, *91*, 4548.
(45) Marr, A. J.; Grieman, F.; Steimle, T. C. *J. Chem. Phys.* **1996**, *105*, 3930.
(46) Rubino, R.; Williamson, J. M.; Miller, T. A. *J. Chem. Phys.* **1995**, *103*, 5964.
(47) Salzberg, A. P.; Applegate, B. E.; Miller, T. A. *J. Mol. Spectrosc.* **1999**, *193*, 434.
(48) Anderson, M. A.; Ziurys, L. M. *Astrophys. J.* **1995**, *452*, L157.
(49) Anderson, M. A.; Ziurys, L. M. *Astrophys. J.* **1996**, *460*, L77.
(50) Anderson, M. A.; Robinson, J. S.; Ziurys, L. M. *Chem. Phys. Lett.* **1996**, *257*, 471.
(51) Xin, J.; Robinson, J. S.; Apponi, A. J., Ziurys, L. M. *J. Chem. Phys.* **1998**, *108*, 2703.
(52) Namiki, K. C.; Steimle, T. C. *J. Chem. Phys.* **1999**, *110*, 11309.
(53) Zhao, C.; Hajigeorgiou, P. G.; Bernath, P. F.; Hepburn, J. W. *J. Mol. Spectrosc.* **1996**, *176*, 268.
(54) Gerkstekorn, S.; Luc, P. *Atlas du Spectre d'Absorption de la Molecule d'Iode*; Laboratoire Aimé-Cotton, CNRS II: Orsay, France, 1978.
(55) Bernath, P. F. Spectroscopy and Photochemistry of Polyatomic Alkaline Earth Containing Molecules; *Advances in Photochemistry*; 1997; Vol. 23, p 1.
(56) Townes, C. H.; Schawlow, A. L. *Microwave Spectroscopy*; Dover Publications Inc.: New York, 1975.
(57) Whitham, C. J.; Beaton, S. A.; Ito, Y.; Brown, J. M. *J. Mol. Spectrosc.* **1998**, *191*, 286.
(58) Pickett, H. M. *J. Mol. Spectrosc.* **1991**, *148*, 371.
(59) Crozet, P.; Ross, A. J.; Linton, C.; Adam, A. G.; Hopkins, W. S.; Le Roy, R. J. *J. Mol. Spectrosc.* **2005**, *229*, 224.
(60) Nakagawa, J.; Wormsbecher, R. F.; Harris, D. O. *J. Mol. Spectrosc.* **1983**, *97*, 37.

(61) Dick, M. J.; Sheridan, P. M.; Wang, J.-G.; Bernath, P. F. *J. Mol. Spectrosc*. **2005**, *233*, 197.
(62) Sheridan, P. M.; Dick, M. J.; Wang, J.-G.; Bernath, P. F. *J. Mol. Spectrosc*. **2005**, *233*, 278.
(63) Marr, A. J.; Tanimoto, M.; Goodridge, D.; Steimle, T. C. *J. Chem. Phys*. **1995**, *103*, 4466.
(64) Lefebvre-Brion, H.; Field, R. W. *The Spectra and Dynamics of Diatomic Molecules*; Elesevier: Amsterdam, The Netherlands, 2004.
(65) Dixon R. N. *Mol. Phys*. **1965** *10* 1.
(66) Hilborn, R. C.; Qingshi, Z.; Harris, D. O. *J. Mol. Spectrosc*. **1983**, *97*, 73.
(67) Brazier, C. R.; Bernath, P. F. *J. Mol. Spectrosc*. **1985**, *114*, 163.